Journal of
Applied Crystallography
ISSN 0021-8898

Received 4 August 2010
Accepted 11 December 2010

Determining the energy-dependent X-ray flux variation of a synchrotron beamline using Laue diffraction patterns

Catherine Dejoie,[a]* Martin Kunz,[a] Nobumichi Tamura,[a] Colin Bousige,[b] Kai Chen,[c] Simon Teat,[a] Christine Beavers[a] and Christian Baerlocher[d]

[a]Advanced Light Source, Lawrence Berkeley National Laboratory, 1 Cyclotron Road, Berkeley, CA 94720, USA, [b]Institut Laue–Langevin, 6 rue Jules Horowitz, 38042 Grenoble Cedex 9, France, [c]Department of Earth and Planetary Sciences, McCone Hall, UC Berkeley, Berkeley, CA 94720, USA, and [d]Laboratorium für Kristallographie, ETH Zürich, Wolfgang-Pauli-Strasse 10, 8093 Zürich, Switzerland. Correspondence e-mail: cdejoie@lbl.gov

Although the spectrum originating from a superconducting bending magnet is quasi-continuous, it shows important intensity variations through its spectral range. A method to determine the incident energy-dependent flux variation based on the comparison between observed intensities and the calculated intensities of a well known structure (calcite) is presented here. It is found that the measured flux is highly sensitive to the use of correct Debye–Waller factors for the atoms of the standard crystal. By using the measured flux curve, it was possible to unambiguously index the Laue diffraction pattern of a trigonal crystal structure in its hexagonal setting. This is a crucial but difficult first step for the determination of strain and stress in materials with this symmetry, such as quartz, Mg, Ti, Zn *etc.*

1. Introduction

One of the advantages of synchrotron X-ray sources is the quasi-continuous nature of the X-ray spectrum provided by their bending magnets and some insertion devices. This allows for energy-tunable X-ray light, enabling a variety of spectroscopic techniques (*e.g.* EXAFS, XANES) but also white-beam X-ray diffraction. The proper characterization of the incident spectrum is important for a valid interpretation of these experiments. Traditionally, flux curves are measured by scanning a monochromator through the white incident beam and recording the energy-dependent flux variation using a scintillator or ion chamber (MacDowell *et al.*, 2001; Kunz *et al.*, 2005, 2009). While this gives an absolute photon count, it does not reflect the true photon flux of the white beam, since it is modulated not only by the reflectivity and Darwin width of the monochromator, but also by the energy-dependent bandwidth, footprint and spillover effect on the monochromator crystals. It is for these reasons that measured and calculated monochromatic flux curves tend to be different from calculated white-beam flux curves (Kunz *et al.*, 2005, 2009; Fig. 1). A more direct method to characterize the flux curve from a quasi-continuous source is therefore desirable.

Evaluation of the incident flux curve using Laue patterns has been reported in protein crystallography. The large unit cells of protein crystals allow the empirical fitting of the incident flux curve by comparing the intensities of symmetry-related reflections occurring simultaneously in a single Laue pattern (Ren *et al.*, 1999; Ren & Moffat, 1995; Helliwell, 1992). The success of this technique is based on the high redundancy of the data set owing to the large unit cells of protein crystals. The application of this method is therefore difficult for inorganic compounds, which have much smaller unit cells and thus a much less densely packed reciprocal space. Gomez de Anderez *et al.* (1989) reported the determination of the incident flux curve prior to structure determination using Laue patterns of a small molecule (chlorofluoroacetamide, space group $P2_12_12_1$, $a = 5.418$, $b = 12.030$, $c = 15.837$ Å). The same method as the one used for protein crystallography was applied. The required statistic was achieved by rotating the crystal to collect the necessary number of independent reflections. While this flux curve determination method has proved to be successful, we address the problem when the rotation of inorganic crystals is impossible, as is found in composite materials or where only very small samples are available.

We present here a method based on the use of a single-crystal Laue X-ray diffraction pattern of a well known crystal. The measured intensities can be analytically corrected for effects caused by absorption, polarization and Lorentz factors as well as harmonic overlap. Comparing the thus pre-corrected measured intensities with the calculated amplitudes of the structure factors for the structurally well characterized standard crystal allows us to extract a white-beam flux curve. While this does not provide us with an absolute photon count, it gives a reliable measure of the relative intensities along the white-beam spectrum. This can be used for incident flux correction on absorption spectra or diffraction intensities. This

Table 1
Atomic coordinates, occupancy and U_{eq} as derived from *SHELX* refinement.

(*a*) Using monochromatic data.

Atoms	*x*	*y*	*z*	Occupancy	U_{eq}
Ca	0	0	0	1	0.0120 (5)
C	0	0	0.25	1	0.0111 (9)
O	0.257 (3)	0	0.25	1	0.0194 (6)

(*b*) Using Laue data.

Atoms	*x*	*y*	*z*	Occupancy	U_{eq}
Ca	0	0	0	1	0.007 (2)
C	0	0	0.25	1	0.007 (3)
O	0.28 (2)	0	0.25	1	0.020 (3)

is also a first and most important step for structure determination and/or structure refinement of inorganic compounds with small lattice parameters using the micro Laue technique. Laue diffraction is a desirable alternative in cases where the classic monochromatic method is inadequate, for example when the sample crystal cannot be rotated, *e.g.* composite materials, crystals embedded in a heterogeneous medium, very small (<5 µm) size crystals or crystals in ancillary equipment.

A Laue diffraction pattern is obtained when a stationary crystal is illuminated by a polychromatic X-ray beam (white or pink beam). The interpretation of diffraction intensities of a Laue experiment is not straightforward (Harding *et al.*, 1988). This is mainly due to two factors. On the one hand, the intensity in a Laue experiment, while being primarily determined by the atomic content of the unit cell, is modulated not only by the incident flux curve but also by a series of other factors such as energy-dependent absorption and X-ray scattering power (Helliwell *et al.*, 1989). On the other hand, harmonically related reflections [*i.e.* reflections originating from parallel sets of lattice planes (*nh nk nl*), *n* = integer] have the same diffraction angle and thus occupy the same point on the area detector (Cruickshank *et al.*, 1987). Commonly used area detectors are blind to the energy of a photon and we therefore only see the sum of all harmonically overlapped peaks, but not their individual contributions. In order for this method to work, we therefore need a structurally well characterized and constrained crystal with a reciprocal lattice sufficiently dense to cover the investigated X-ray spectrum with non-overlapping peaks.

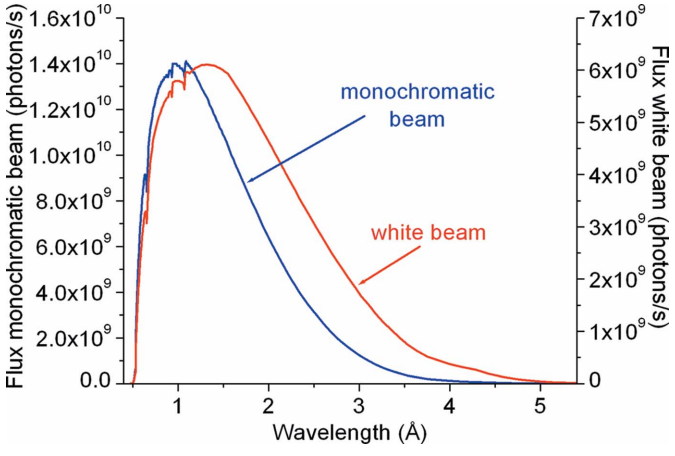

Figure 1
Comparison between the theoretical calculated flux curve for beamline 12.3.2 using a monochromatic beam and a white beam. Theoretical flux curves were calculated using *SHADOW* (Lai & Cerrina, 1986) based on the characteristics of the beamline and monochromator parameters for a four-bounce Si(111) channel-cut monochromator as described by Kunz *et al.* (2009). The main differences between the two theoretical incident flux curves occur at high wavelength (*i.e.* low photon energy) values.

2. Methods

2.1. Sample

In order to calibrate a flux curve against a set of calculated structure factors, we need a crystal with a well known structure with little variability. The crystal must be chemically stable enough to withstand a white synchrotron X-ray beam. Lastly, the crystal should be free of imperfections but show enough mosaic spread to avoid significant extinction damage. A gem-quality crystal of calcite made a good standard crystal. Its three atoms in the asymmetric unit have only one free positional parameter in addition to the displacement parameters (see below). The crystal was provided by Professor R. Wenk (UC Berkeley). To obtain the best possible structure factors for this specific crystal, structure factors of the very same sample that served as standard crystal were measured using monochromatic X-ray diffraction. The quartz sample used to illustrate the possibility of indexing the trigonal lattice was also provided by Professor R. Wenk, along with a plagioclase sample (sanidine, space group *C*2/*m*, a = 8.583, b = 13.007, c = 7.194 Å) to test the accuracy of the data correction.

2.2. Data collection

Monochromatic single-crystal data of calcite were collected on beamline 11.3.1 at the Advanced Light Source (ALS) of the Lawrence Berkeley National Laboratory (LBNL), on a Bruker AXS APEXII CCD diffractometer. A calcite crystal (50 × 40 × 20 µm) in inert oil was mounted on a glass fiber. Si(111)-monochromated radiation of wavelength λ = 0.7749 (1) Å was used. Structure solution and refinement of the calcite structure were carried out using the *SHELX* package (Sheldrick, 2008) ($CaCO_3$, trigonal, space group No. 167, $R\bar{3}c$, T = 293 K, $a = b$ = 4.997 (2), c = 17.081 (9) Å, Z = 6, 1746 reflections measured, R_{int} = 0.0403, 128 unique reflections, $R1$ = 0.0382 for observed data and $wR2$ = 0.0920 for all data; Table 1*a*).

Laue X-ray microdiffraction data were measured on beamline 12.3.2 at the ALS (LBNL). A high-brilliance synchrotron polychromatic X-ray beam (5–24 keV) was focused down to about 1 µm^2 by a pair of Kirkpatrick–Baez mirrors (Kunz *et al.*, 2009). The very same sample measured on beamline 11.3.1 was mounted on the sample stage, which was tilted by 45° relative to the incoming beam (Fig. 2). Laue diffraction patterns were recorded using a MAR 133 X-ray

CCD detector, positioned at a 90° angle with respect to the incident X-ray beam. The diffraction geometries, including the distance from the CCD to the sample (~78 mm), the center position of the CCD and the CCD tilt angles, were calibrated by indexing a diffraction pattern of the practically strain free calcite sample. All diffraction patterns were indexed using the *XMAS* software package (Tamura *et al.*, 2003). For each peak of integrated intensity $I_{\rm int}$ indexed on the Laue pattern, indices of the reflection $H = (hkl)$, its associated energy E and the diffraction angle 2θ were generated. The raw Laue intensities were scaled using the correction factors detailed in the next section.

2.3. The 'reverse method' to determine a white X-ray spectrum

The 'reverse method' is based on comparing the calculated structure factors of a well known standard crystal with the measured intensities diffracted by the standard crystal off the incident white beam (Laue diffraction).

The diffracted intensity of a spot M of a Laue pattern is the sum of the squared structure factors (F) over all the allowed harmonics, multiplied by a scaling factor $f_{\rm corr}(M, \lambda_i)$:

$$I(M) = \sum_{\substack{\text{harmonics}\\ i=1..n}} f_{\rm corr}(M, \lambda_i)\, F^2(h_i, k_i, l_i, \lambda_i, \theta, \text{crystal}), \qquad (1)$$

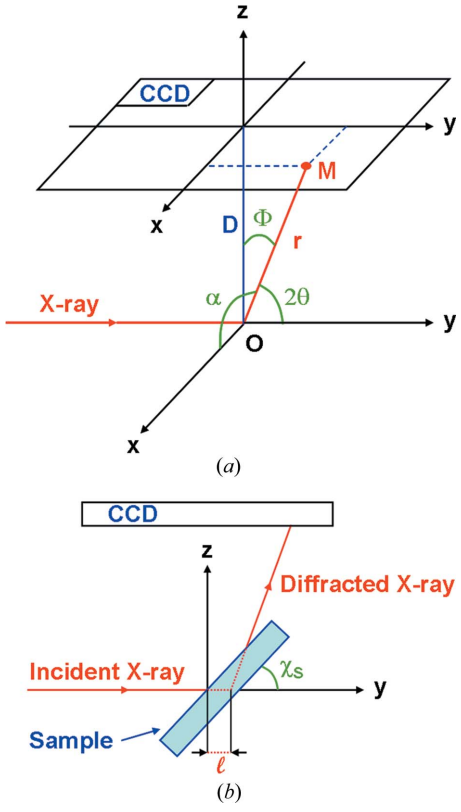

Figure 2
(*a*) Geometry of the Laue measurement on beamline 12.3.2. (*b*) Illustration of the sample absorption in reflection geometry.

$$f_{\rm corr}(M, \lambda_i) = f_{\rm scale}\, f_{\rm absorption}(M, \lambda_i)\, f_{\rm Lorentz}(M, \lambda_i) \times f_{\rm polarization}(M)\, f_{\rm flux}(\lambda_i)\, f_{\rm detector}(M, \lambda_i). \qquad (2)$$

The differences of the detector response $f_{\rm detector}(M, \lambda_i)$ as a function of the position of the spot M on the detector (in relation to the geometry of the experiment) at a given wavelength are taken into account by applying dark-current, flat-field and spatial-distortion corrections to the raw Laue images. The method presented here enables extraction of the normalization curve *versus* the energy, $f_{\rm norm}(\lambda_i)$, which corresponds to the convolution of the detector response $f^{\rm corr}_{\rm detector}(\lambda_i)$ with the incident flux $f_{\rm flux}(\lambda_i)$. The extraction of the normalization curve $f_{\rm norm}(\lambda_i)$ by the reverse method requires that the structure factor is properly corrected for each harmonic for all angle- and energy-dependent modulation factors affecting the individual harmonic reflection [equation (2)]. Factors taken into consideration are an angle- and energy-dependent absorption correction $f_{\rm absorption}(M, \lambda_i)$, an angle- and energy-dependent Lorentz factor $f_{\rm Lorentz}(M, \lambda_i)$, and an angle-dependent polarization correction $f_{\rm polarization}(M)$. In the following we give a brief description of each of these correction factors.

(*a*) Harmonic deconvolution and structure factor calculation. Indexing of the Laue pattern reveals energy (E) and Miller indices (hkl) for each reflection. The occurrence of harmonic overlap is tested in a very straightforward way: the generic reflection $H_0 = (h/m\ k/m\ l/m)$ and the associated energy E/m are determined (m stands for the greatest common divisor of h, k and l). The possibility of existence of $H_m = mH_0$ is then tested, following the conditions that Em must be between $E_{\rm min} = 5$ keV and $E_{\rm max} = 24$ keV (the energy range available at the beamline), and that the indices must satisfy the reflection conditions applicable for the particular space group. The structure factor is then calculated for each harmonic using equation (3), where N stands for the number of atoms in the unit cell, whose positions in direct space are (x_j y_j z_j). The atomic scattering factor $f_i(\lambda_n, \theta_n)$, is calculated using the analytical expression given in equation (4) [a, b and c represent element-specific Cromer–Mann coefficients as listed in *International Tables for Crystallography* (2004, Vol. C)]. The term $\exp[-8\pi^2 U_j(\sin\theta_n/\lambda_n)^2]$ represents the Debye–Waller factor, with U_j the isotropic displacement parameter of the atom j.

$$F(h_n, k_n, l_n, \lambda_n, \theta_n) = \sum_{j=1}^{N} \left\{ f_j(\lambda_n, \theta_n) \exp\left[2i\pi(h_n x_j + k_n y_j + l_n z_j)\right] \times \exp\left[-8\pi^2 U_j(\sin\theta_n/\lambda_n)^2\right] \right\}, \qquad (3)$$

$$f_j(\lambda_n, \theta_n) = c_j + \sum_{q=1}^{4} a_{jq} \exp\left[-b_{jq}(\sin\theta_n/\lambda_n)^2\right]. \qquad (4)$$

(*b*) Absorption. Diffracted X-ray beams are absorbed within the sample and in the air path between sample and detector [equation (5)]. The air absorption and the sample absorption are path and energy dependent. They can be

corrected analytically for a given experimental setup, once we know the energy for each diffraction spot M (*i.e.* the pattern is indexed). Correction for sample absorption is given in equation (6). ρ_S stands for the sample density and $(\mu/\rho)_S$ the mass attenuation coefficient (depending on λ_n) calculated from each element i of the sample [$(\mu/\rho)_S = \sum_i w_i(\mu/\rho)_i$, with w_i denoting the mass fraction of the element i]. D is the sample–detector distance, x and y are the coordinates of the spot M in the detector coordinate system, and χ_S is the angle between the incoming beam and the sample surface (Fig. 2*b*). L_{max} represents the maximum path length of the incoming beam in the sample: L_{max} is calculated to be equal to the larger of the attenuation length or the thickness of the sample. In reflection geometry (Fig. 2), most of the diffraction originates from the sample surface. As calcite is not constituted by strongly absorbing atoms, in the first approximation, the sample absorption can be neglected. In the present case, introduction of the absorption correction in the calculation contributes less than 5% of the corrected structure factor values. That is why we only took air absorption into account in the following [equation (7)]. In equation (7), $x = \rho_{air} r$ stands for the mass thickness, ρ_{air} the air density, r the length of the air path and μ/ρ the mass attenuation coefficient (depending on λ_n).

$$f_{absorption}(M, \lambda_n) = f^{air}_{absorption}(M, \lambda_n) f^{sample}_{absorption}(M, \lambda_n), \quad (5)$$

$$f^{sample}_{absorption}(M, \lambda_n) = \int_{l=0}^{l=L_{max}} \exp\left(-\rho_S \left(\frac{\mu}{\rho}\right)_S \left\{ l + \frac{l \tan \chi_S}{(y-l)\tan \chi_S - D} \times \left[x^2 + (y-l)^2 + D^2\right]^{1/2} \right\} \right), \quad (6)$$

$$f^{air}_{absorption}(M, \lambda_n) = \exp(-x\mu/\rho). \quad (7)$$

(*c*) Lorentz factors. Although in Laue diffraction the sample is stationary and thus does not move through the Ewald sphere, there is still a Lorentz correction to be applied, since the density of Ewald spheres that a reflection intersects is dependent on the distance $R = 1/d_{hkl}$, d_{hkl} being the lattice spacing. We used the Lorentz correction proposed by Kalman (1979) for a stationary sample in a polychromatic beam [equation (8)].

$$f_{Lorentz}(M, \lambda_n) = \frac{\lambda_n^2}{2\sin^2\theta_n}. \quad (8)$$

(*d*) Polarization factor. The horizontal polarization of the synchrotron beam leads to a diffraction-angle-dependent attenuation for horizontal scattering vectors relative to scattering vectors perpendicular to the polarization plane. This effect can also be corrected for analytically and is independent of the energy [equation (9)]. In equation (9), D stands for the sample–detector distance, x and y are the coordinates of the spot M in the detector coordinate system, and r is the distance between the sample and spot M (Fig. 2*a*). The p parameter has been refined by least-squares fitting to the value of 0.

$$f_{polarization}(M) = \sin^2\alpha + p\sin^2\Phi = \frac{D^2 + y^2}{r^2} + p\frac{x^2 + y^2}{r^2}. \quad (9)$$

After proper harmonic deconvolution and applying the above-described correction factors to the observed intensities, the normalization curve $f_{norm}(\lambda_i)$ was obtained from equations (1) and (2) by a least-squares fit of an eighth-degree polynomial function to the calculated structure factors. The integrated intensities I_{int} were extracted from the calcite Laue patterns using a 'box method' (*XMAS*; Fig. 3), and theoretical structure factors were calculated using the structural model refined from monochromatic single-crystal data. The error calculated for each point of the incident flux is given by equation (10). The standard deviation $\sigma(I_{int})$ representing the uncertainty on the intensity measurement was calculated from 500 patterns taken in the same conditions on the same point of the sample.

$$\Delta f^{eff}_{flux} = f^{eff}_{flux}\left\{\left[\frac{\sigma(I_{int})}{I_{int}}\right]^2\right\}^{1/2}. \quad (10)$$

3. Results and discussion

The normalization curve $f_{norm}(\lambda_i)$ determined from a single orientation of the standard calcite crystal by the reverse method is shown in Fig. 4(*a*). The most sensitive parameter affecting the quality of the extracted beam spectrum was found to be the U_j values of the standard crystal. As shown in Fig. 4(*b*), the isotropic displacement parameters have to be carefully refined to obtain a meaningful fit. This is because of the strong dependence of the Debye–Waller factor on $\sin\theta/\lambda$. In Fig. 4(*c*), we plot the calculated Debye–Waller factor for the three calcite atoms using the refined U_j values from mono-

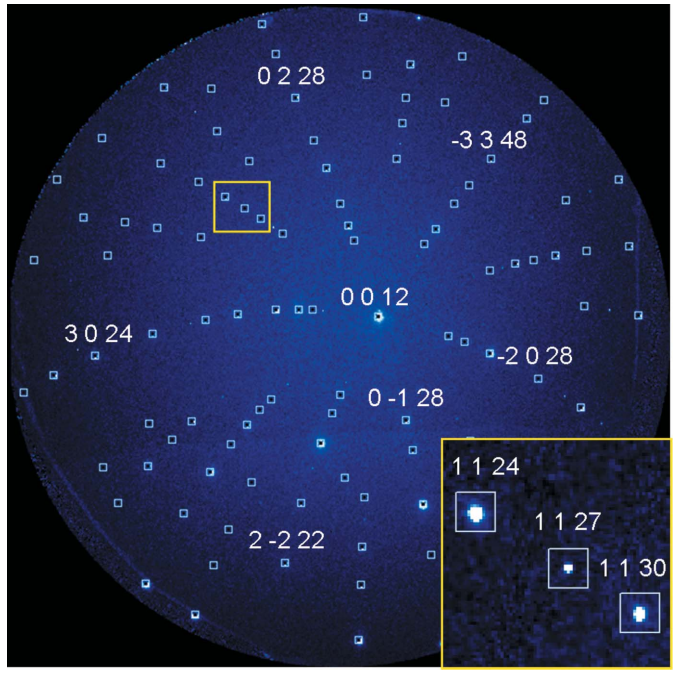

Figure 3
Indexation of a calcite pattern with *XMAS*.

chromatic single-crystal data. For the energy range and the θ values covered, we observe a variation by an order of magnitude between the highest and the lowest Debye–Waller values. This is because of the particular high-angle geometry usually employed for Laue diffraction experiments with the detector placed at $2\theta = 90^\circ$. The Debye–Waller factor also depends on the atom species involved. The U value for the O atom is larger than those for the Ca and C atoms [U(O) = 0.0194 (6), U(C) = 0.0111 (9), U(Ca) = 0.0120 (5) Å^2; Table 1*a*]. This difference is large enough to have a significant effect on the structure factor calculation.

The flux curve measured in this way actually represents a convolution of the incident flux and the energy-dependent detector response. While this is sufficient for most applications, where a normalized flux curve is sought, the proper flux curve can be obtained by subtracting the separately measured detector response. Measurement of the detector response in the 6–12 keV energy range has been achieved by comparing the intensity of the direct beam measured on the CCD detector with that collected with a calibrated pin diode (Fig. 5). Although it is known that the efficiency of the MAR CCD decreases at higher energy, the chromatic dependence of the detector response does not vary significantly within the measured energy range (6–12 keV).

Our measured normalization curve shows differences with the theoretical calculated incident flux (Fig. 4*a*). We attribute this to the incomplete model of the beamline taken into account in the calculation, which omits in particular the presence of beryllium windows, the air path of the beam, and the non-perfect optical elements for the low-energy range and the low detector efficiency for the high-energy range. This supports the need to have an experimental way to determine the incident white-beam flux.

The transferability of the correction factors in particular with respect to the above-determined normalization curve was tested using a data set extracted from a single pattern collected from each of the three following samples: calcite ($CaCO_3$), quartz (SiO_2) and sanidine ($KAlSi_3O_8$). The accuracy of the corrections is given by the R-factor value calculated using the following definition:

$$R = \frac{\sum \left| I_{\rm int}{\rm corr} - S F^2 \right|}{\sum I_{\rm int}{\rm corr}}, \qquad (11)$$

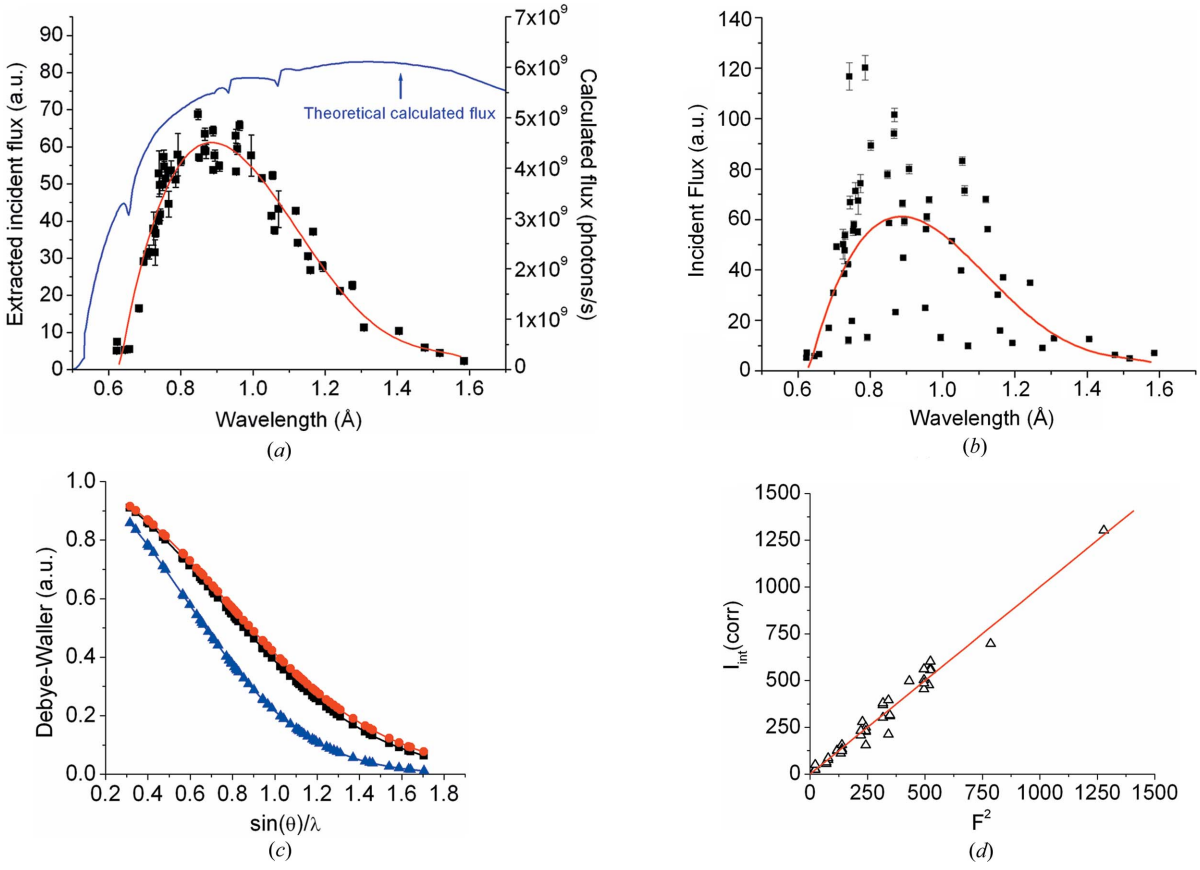

Figure 4
(*a*) Normalization curve determined from one single Laue diffraction pattern of calcite ($CaCO_3$) using the structure factors determined from monochromatic data. The theoretical calculated incident white-beam flux given in Fig. 1 is also displayed for comparison. (*b*) Effect of incorrectly determined displacement parameters [U(Ca) = U(C) = U(O) = 0.01 Å^2]. Owing to the high $\sin\theta/\lambda$ generally found in Laue diffraction experiments, displacement parameters have a very strong influence on the structure factors. The normalization curve determined in (*a*) is also drawn as a reference. (*c*) Evolution of the Debye–Waller factor calculated from monochromatic data as a function of $\sin\theta/\lambda$ for calcite (filled triangles: O atom; filled squares: Ca atom; filled circles: C atom). (*d*) Corrected Laue intensities *versus* calculated structure factors. The strong linear correlation is an indication of the quality of the corrections applied to the Laue data.

Table 2
R factor [equation (11)] calculated from one Laue orientation using reflections without harmonics for calcite, quartz and sanidine samples, depending on the corrections applied.

Sample		Calcite	Quartz	Sanidine
Measured reflections without harmonics in the 5–24 keV range		42	23	86
R factor	Without any correction	0.70	0.67	0.38
	Without incident flux correction	0.25	0.22	0.16
	With all corrections	0.08	0.09	0.11

with S being the scale factor. The results are given in Table 2. The corrected intensities ($I_{\rm int}$corr) as a function of the structure factor (F^2) for reflections without harmonics in the 5–24 keV range for the calcite sample are plotted in Fig. 4(*d*). The final calculated *R*-factor values of about 8, 9 and 11% for calcite, quartz and sanidine, respectively, provide an accuracy limit if intensities from a thus corrected Laue pattern were to be utilized for structure solution and refinement. The effect of the incident flux correction for all the samples is clearly demonstrated with the improvement of the *R* factor by more than 15% for calcite, 13% for quartz and 5% for sanidine.

Despite the low number of non-overlapping reflections extracted from only one orientation of calcite, we attempted to refine the structural model of calcite against the Laue-corrected data using *SHELXL*. The refinement details are given in Table 3, and the final structure of calcite in Table 1(*b*). Refinement was successfully carried out using 18 unique reflections for five refineable parameters, for a final figure of merit $R1 \simeq 7\%$. The high standard deviation values are attributed to the low coverage of the reciprocal space and the small ratio between the number of unique reflections and the number of parameters to refine. The differences in the values of $U_{\rm eq}$ obtained after refinement using the white-beam and monochromatic data are attributed to the lower accuracy of the Laue data compared to the monochromatic data, but remain within 3σ. Complete structure refinement of inorganic compounds after data correction using the normalization curve determined in the present paper will be the subject of a future publication.

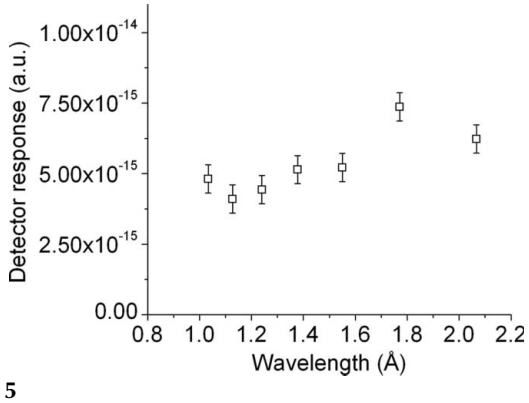

Figure 5
Detector response of the MAR CCD between 6 and 12 keV (1.03–2.06 Å) measured by taking the ratio of the intensity of the direct beam measured on the CCD detector to that collected with a calibrated pin diode.

Table 3
Refinement details of calcite from X-ray Laue data.

Measured reflections (without harmonic)	42
Unique reflections	18
$R_{\rm int}$	0.0752
Number of variables	5
$R1$ for $F_{\rm o} > 4\sigma(F_{\rm o})$	0.069
$R1$ all data	0.069
$wR2$	0.211

$R_{\rm int} = \sum |F_{\rm o}^2 - F_{\rm o}^2({\rm mean})| / \sum F_{\rm o}^2$, $R1 = \sum ||F_{\rm o}| - |F_{\rm c}|| / \sum |F_{\rm o}|$ and $wR2 = \{\sum[w(F_{\rm o}^2 - F_{\rm c}^2)^2] / \sum[w(F_{\rm obs}^2)^2]\}^{1/2}$.

A first applicable benefit of correctly assessing intensities of Laue diffraction patterns is the ability to properly index Laue diffraction patterns of a primitive trigonal lattice, *i.e.* a trigonal lattice in a hexagonal setting. One of the main applications of Laue diffraction is the determination of strain and stress tensors with high spatial resolution of various materials. Lattices of trigonal symmetry show a hexagonal pseudo-symmetry in their diffraction patterns. Reflections of lattice planes such as $\{10\bar{1}0\}$ and $\{1\bar{1}00\}$ have identical d spacings but different structure factors. Since the elastic constant of a trigonal lattice may differ greatly between the $\langle 10\bar{1}0\rangle$ and $\langle 01\bar{1}0\rangle$ directions, the correct indexing of a Laue pattern is required to evaluate stress states. The indexing needs to be correct at the first attempt since this application relies on the indexing of 10^3–10^4 patterns. An indexing algorithm that does not take into account the diffracted intensities can thus not differentiate between these two reflections. This is the case for most of the Laue indexing software (Jacobson, 1986; Chung & Ice, 1999; Gupta & Agnew, 2009). This results in a 60° orientation ambiguity when indexing a primitive trigonal lattice. The indexing algorithm finds randomly one of two possible non-equivalent orientations, (hkl) or $(h'k'l')$, with $h' = h + k$, $k' = -h$, $l' = l$. By comparing the calculated structure factor of each reflection of the two possible indexations with the corrected intensities, the correct orientation can be unambiguously assigned. Fig. 6 shows corrected intensities ($I_{\rm int}$corr) as a function of structure factor (F^2) for a quartz sample (space group No. 154, $P3_221$) for each of the two possible orientations. Only peaks without harmonics in the 5–24 keV range are plotted. One clearly sees a strong linear relation between $I_{\rm int}$corr and F^2 for the second indexing possibility (Fig. 6*b*), whereas the alternative orientation shows very poor correlation between corrected intensities and calculated structure factors (Fig. 6*a*).

4. Outlook

The reverse method presented here is to the best of our knowledge the most direct way to measure the spectrum of a white X-ray source. The fact that it yields a convolution of detector response and actual X-ray spectrum is advantageous for most applications, such as the corrections of Laue diffraction intensities for the purpose of structure solution and refinement. By independently assessing the detector response, this method can also be used as a characterization tool for

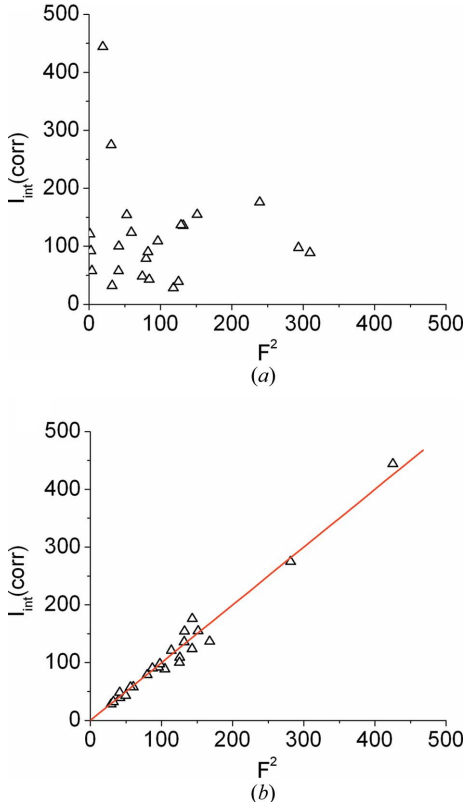

Figure 6
Example of the effect of a wrong indexing of a trigonal lattice (quartz) on the extracted intensities. (*a*) 'Wrong' orientation, (*b*) correct orientation. A properly applied incident flux correction allows for the discrimination between two non-equivalent but otherwise indistinguishable indexings.

quasi-continuous X-ray sources such as synchrotron bending magnets and wigglers.

The ability to measure white-beam incident flux spectra will allow the use of Laue diffraction also for inorganic materials. Traditionally, this technique has only been used in exceptional cases for very large unit cell crystals as found in protein crystallography. In these cases, the high redundancy of data allows one to refine simultaneously the incident spectrum and the crystal structure of the sample investigated. This is not possible for inorganic compounds, which have much smaller unit cells and thus a much less densely packed reciprocal space. The ability to characterize the incident spectrum will allow the use of the Laue diffraction technique to be expanded to cases in materials science where traditional monochromatic X-ray diffraction is unpractical. Examples for such cases are crystals enclosed in bulky ancillary equipment (*i.e.* reaction flow cells, high-pressure cells) or inseparably intergrown composite materials.

We acknowledge the help of J. M. Glossinger who performed the calculation of the monochromatic and the white-beam incident flux curve. The Advanced Light Source is supported by the Director, Office of Science, Office of Basic Energy Sciences, Materials Science Division, of the US Department of Energy under contract No. DE-AC02-05CH11231 at Lawrence Berkeley National Laboratory. The microdiffraction program at the ALS on beamline 12.3.2 was made possible by NSF grant No. 0416243.

References

Chung, J. S. & Ice, G. E. (1999). *J. Appl. Phys.* **86**, 5249–5255.
Cruickshank, D. W. J., Helliwell, J. R. & Moffat, K. (1987). *Acta Cryst.* A**43**, 656–674.
Gomez de Anderez, D., Helliwell, M., Habash, J., Dodson, E. J., Helliwell, J. R., Bailey, P. D. & Gammon, R. E. (1989). *Acta Cryst.* B**45**, 482–488.
Gupta, V. K. & Agnew, S. R. (2009). *J. Appl. Cryst.* **42**, 116–124.
Harding, M. M., Maginn, S. J., Campbell, J. W., Clifton, I. & Machin, P. (1988). *Acta Cryst.* B**44**, 142–146.
Helliwell, J. R. (1992). *Macromolecular Crystallography with Synchrotron Radiation.* Cambridge University Press.
Helliwell, J. R., Habash, J., Cruickshank, D. W. J., Harding, M. M., Greenhough, T. J., Campbell, J. W., Clifton, I. J., Elder, M., Machin, P. A., Papiz, M. Z. & Zurek, S. (1989). *J. Appl. Cryst.* **22**, 483–497.
Jacobson, R. A. (1986). *J. Appl. Cryst.* **19**, 283–286.
Kalman, Z. H. (1979). *Acta Cryst.* A**35**, 634–641.
Kunz, M. *et al.* (2005). *J. Synchrotron Rad.* **12**, 650–658.
Kunz, M. *et al.* (2009). *Rev. Sci. Instrum.* **80**, 035108.
Lai, B. & Cerrina, F. (1986). *Nucl. Instrum. Methods Phys. Res. Sect. A*, **246**, 337–341.
MacDowell, A. A., Celestre, R. S., Tamura, N., Spolenak, R., Valek, B., Brown, W. L., Bravman, J. C., Padmore, H. A., Batterman, B. W. & Patel, J. R. (2001). *Nucl. Instrum. Methods Phys. Res. Sect. A*, **467**, 936–943.
Ren, Z., Bourgeois, D., Helliwell, J. R., Moffat, K., Šrajer, V. & Stoddard, B. L. (1999). *J. Synchrotron Rad.* **6**, 891–917.
Ren, Z. & Moffat, K. (1995). *J. Appl. Cryst.* **28**, 461–481.
Sheldrick, G. M. (2008). *Acta Cryst.* A**64**, 112–122.
Tamura, N., MacDowell, A. A., Spolenak, R., Valek, B. C., Bravman, J. C., Brown, W. L., Celestre, R. S., Padmore, H. A., Batterman, B. W. & Patel, J. R. (2003). *J. Synchrotron Rad.* **10**, 137–143.